IEEE Access
Multidisciplinary ⋮ Rapid Review ⋮ Open Access Journal

Received March 5, 2020, accepted March 21, 2020, date of publication April 2, 2020, date of current version May 13, 2020.

Digital Object Identifier 10.1109/ACCESS.2020.2985294

Broadband Circularly Polarized Rectenna With Wide Dynamic-Power-Range for Efficient Wireless Power Transfer

ZHI-XIA DU[1], (Member, IEEE), SHAO FEI BO[1], YUN FEI CAO[1,2], (Member, IEEE), JUN-HUI OU[1], (Member, IEEE), AND XIU YIN ZHANG[1], (Senior Member, IEEE)

[1]School of Electronic and Information Engineering, South China University of Technology, Guangzhou 510641, China
[2]State Key Laboratory of Millimeter Waves, Nanjing 210096, China

Corresponding author: Yun Fei Cao (caoyf@scut.edu.cn)

This work was supported in part by the National Natural Science Foundation of China under Grant 61725102 and Grant 61701182, in part by the Open Research Program from the State Key Laboratory of Millimeter Waves under Grant K201801, and in part by the Project funded by China Postdoctoral Science Foundation under Grant 2018T110866.

ABSTRACT This paper presents a circularly polarized (CP) rectenna with the advantage of achieving high efficiency in both wide operating power and frequency ranges. The proposed rectenna is composed of a high-efficiency rectifier and broadband CP antenna. In the proposed rectifier, a novel wideband resistance compression technique is presented, highly improving the matching performance of the circuit in a wide range of input power and frequency. The technique is achieved by an impedance manipulation network and a coupled-lines-based resistance compression network (RCN). Theoretical analysis is carried out and closed-form equations are derived for the design of the rectifier. Simulated and measured results show that over 60% (up to 76%) conversion efficiency is achieved for the input power range of 5-17 dBm and frequency band of 1.7-2.9 GHz (mobile, Wi-Fi and ISM bands). Subsequently, unlike the conventional half-wavelength slot antenna, a compact CP antenna with a side length of quarter wavelength is designed by using a 1-wavelength loop slot and a coupled-line-based phase shifter. It has wide axial-ratio bandwidth and good radiation pattern. At last, by integrating the proposed rectifier together with the CP slot antenna, a broadband CP rectenna is completed with higher efficiency by about 18.6% than that without wideband RCN.

INDEX TERMS Broadband rectenna, wideband resistance compression technique, dynamic power range, wireless power transfer.

I. INTRODUCTION

Recently, wireless power transfer (WPT) has gained increasing attention. It is very significant in many applications, such as internet of things (IoT) devices [1], medical devices [2], low-power electronics [3], and simultaneous wireless information and power transfer (SWIPT) system [4], [5]. At the receiver side of both WPT and SWIPT system, the efficiency improvement of the RF rectennas is an important work.

On the one hand, achieving high efficiency in wide or multiple frequency bands is beneficial for many applications, including increasing the output power of the rectenna for energy harvesting [6]–[12] and using the high peak-to-average power ratio (PAPR) signals [13]–[16]. Broadband rectennas are necessary for the PAPR signals such as UWB signals and chaotic signals [17], [18]. Moreover, broadband design also improves the applicability of WPT for the applications at different countries and regions with different requirements about working frequency band. In [19], a multiband rectenna with shorting pins eliminating the matching network is introduced, the frequency bands cannot be tuned independently. Besides, circular-polarization also enables the antenna to receive more energy from the complex environment with multipath reflection and refraction. Nevertheless, it is challenging to design circularly-polarized rectennas in wide bandwidth.

On the other hand, it is also important to maintain high efficiency within a wide dynamic power range. The variation of the power levels leads to diode impedance change due to the characteristic of non-linearity, and then causes impedance

The associate editor coordinating the review of this manuscript and approving it for publication was Tariq Masood.

mismatch and rectifier performance degradation. In order to solve this problem, high-efficiency rectifiers within wide power range are implemented [20]–[25]. Among these works, some of the rectifiers with wide operating power range are designed by connecting several sub-rectifiers optimized at different incident power levels together in parallel [20]–[22]. But extra power management systems are needed which increases the circuit complexity. Varactor diodes [23] and GaAs pHEMT [24] are used to improve the matching performance and extend the maximum breakdown power. A branch-line coupler is designed to re-inject the reflected power due to impedance mismatch back into the sub-rectifiers, which improves the conversion efficiency [25]. However, these methods cause additional energy loss.

To reduce the cost for extending the operating power range, resistance compression networks (RCNs) are applied to rectifier designs [26]–[30]. In the previous RCN-based rectifiers [26]–[30], the RCN compresses the variation range of the rectifier input resistance which changes with input power, consequently improving the matching and conversion efficiency. However, most of the reported RCN-based rectifiers have limited operating frequency bandwidth since the performance of RCNs heavily relies on the working frequency of the network, including the auxiliary circuit that transforms the diode impedance to be resistive, and the transmission line RCN in [29]. When the frequency varies, the RCN cannot maintain its function since it is frequency-dependent. Therefore, a wideband impedance manipulation and resistance compression technique is necessary to match the rectifying circuit with the broadband CP antenna. In [31], a complex impedance compression network is developed and applied to the single- and dual-band rectifiers, but has narrow operating frequency bandwidth. In [32], a wideband rectifier is designed by using hybrid resistance compression technique. However, the operating power range is not enhanced.

In this paper, a broadband circularly polarized (CP) rectenna with wide operating power range is proposed. It consists of a wideband RCN-based rectifier and a CP antenna. Unlike the previous frequency-dependent RCN which can only maintain its function in a fixed frequency band, a novel wideband resistance compression technique is proposed in this paper. This technique can simultaneously improve the matching of the rectifier within wide input power and frequency ranges. It is realized by an impedance manipulation network and a coupled-lines-based resistance compression network (RCN). By using this technique, the diode impedance changing with the input power and frequency can be compressed, and the conversion efficiency of the rectifier can be enhanced. A compact broadband CP antenna is designed by feeding a single $1-\lambda$ loop-shaped radiating slot through a wideband coupled-line-based phase shifter. Thus the proposed CP antenna has wide axial-ratio bandwidth and good radiation pattern with a very compact size. At last, the rectifier is co-designed with the CP antenna to complete a CP rectenna with the advantage of high efficiency in both wide operating power and frequency ranges. The proposed CP rectenna can fulfil the requirements of different countries in different frequency bands. Experimental verification using a WPT experiment system shows that the rectenna has good performance.

II. WIDEBAND RESISTANCE COMPRESSION TECHNIQUE FOR RECTIFIERS

A high-efficiency rectifier based on a novel wideband RCN is designed in this section. As shown in Fig. 1, the proposed rectifier is composed of an impedance transformer (TL7), a coupled-lines-based wideband RCN, two identical impedance manipulation networks, diodes and filtering capacitors. The impedance manipulation networks firstly convert the complex impedance to resistance in a wide band. Then the wideband RCN reduces the variation range of the resistance and TL7 converts the resistance range to be around 50 Ω. The configuration of the impedance manipulation network and wideband RCN are described and the design formulas are derived to guide the design. The paralleled capacitor in each branch is used to redirect the RF signals back to the diode, as well as transmitting the DC power to the load R_{Load}. In this design, the Schottky diode HSMS-2860 with the SOT-23 Package is used. The filtering capacitor C from Murata has a value of 100 pF, and the load resistance is 510 Ω.

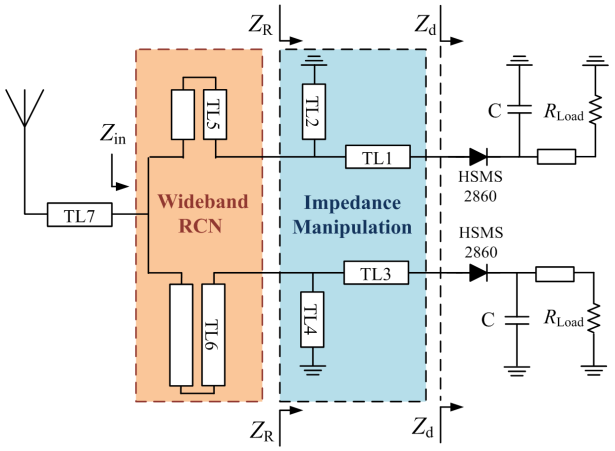

FIGURE 1. Diagram of the proposed broadband RCN-based rectifier.

The simulated and measured results including the return loss and conversion efficiency of the proposed rectifier are discussed and compared with some counterparts, as well as other related works.

A. IMPEDANCE MANIPULATION NETWORK

The calculation procedure of the parameters of both two impedance manipulation networks are described in this part. The impedance manipulation networks on the two branches are exactly the same. Each one consists of a microstrip line (TL1 or TL3) and a short-circuited shunt stub (TL2 or TL4). It is used to transform the input impedance of the rectifying circuit to be nearly resistive within the operating input power

and frequency range. Because the two impedance manipulation networks are the same, only the one with TL1 and TL2 is analyzed here as an example.

1) SERIES TRANSMISSION LINE TL1

Firstly, the characteristic impedance Z_1 and electrical length θ_1 of TL1 are calculated. TL1 is used to make the imaginary part of the diode impedance Z_L odd-symmetrical with respect to the center frequency, meanwhile maintaining the real part nearly constant. In the operating frequency band from f_1 to f_2, the diode input impedances Z_d at the boundary frequency f_1 and f_2 are denoted as $R_{d1}+jX_{d1}$ and $R_{d2}+jX_{d2}$, respectively. The characteristic impedance and electrical length of TL1 are Z_1 and $\theta(f_1)$ (or θ_1) at f_1. By using TL1, the input impedance at f_1 and f_2 can be expressed as

$$Z_{in1}(f_1) = Z_1\frac{(R_{d1}+jX_{d1})+jZ_1\tan\theta(f_1)}{Z_1+j(R_{d1}+jX_{d1})\tan\theta(f_1)} \quad (1)$$

$$Z_{in1}(f_2) = Z_1\frac{(R_{d2}+jX_{d2})+jZ_1\tan\theta(f_2)}{Z_1+j(R_{d2}+jX_{d2})\tan\theta(f_2)}. \quad (2)$$

where $\theta(f_2)$ is the electrical length at f_2. By introducing the frequency ratio $k = f_2/f_1$, we have $\theta(f_2) = k\theta(f_1) = k\theta_1$. Moreover, TL1 transforms the input impedances $Z_{in1}(f_1)$ and $Z_{in1}(f_2)$ to be conjugated, that is, $Z_{in1}(f_1) = [Z_{in1}(f_2)]^*$. Therefore, Z_1 and θ_1 can be calculated by

$$Z_1 = \sqrt{R_{d1}R_{d2}+X_{d1}X_{d2}+\frac{X_{d1}+X_{d2}}{R_{d2}-R_{d1}}(R_{d1}X_{d2}-R_{d2}X_{d1})} \quad (3)$$

$$\theta_1 = \frac{1}{1+k}\{\arctan[\frac{Z_1(R_{d1}-R_{d2})}{R_{d2}X_{d1}-R_{d1}X_{d2}}]+n\pi\} \quad (n=1,2\ldots.). \quad (4)$$

The diode input impedance Z_d can be obtained by circuit simulation. Then the characteristic impedance Z_1 and electrical length θ_1 of TL1 can be calculated according to (3) and (4). In this design, the working band of the rectifier is expected to be [1.7 GHz, 2.7 GHz]. Then Z_1 and θ_1 are calculated to be 140.4 Ω and 45.5°, respectively. Fig. 2(a) shows the input impedance Z_{in1} of the rectifying circuit in the frequency band of 1.7-2.7 GHz. As observed, the real part of Z_{in1} is around 39 Ω and the imaginary part is nearly odd-symmetrical with respect to the frequency of 2.2 GHz at the input power level of 12 dBm. Moreover, the impedance Z_{in1} at 0 dBm and 6 dBm varies in a similar trend with that at 12 dBm, and the curves are quite close to each other, benefiting from TL1. Thus TL1 still works, although the diode impedance changes with input power.

2) SHUNT SHORTED-CIRCUITED LINE TL2

Secondly, the characteristic impedance Z_2 and electrical length θ_2 of TL2 are calculated. TL2 is used to offset the imaginary part of Y_{in1} maintaining the real part nearly unchanged. Y_{in1} is the inverse of Z_{in1}. The characteristic impedance and electrical length of TL2 are Z_2 and $\theta(f_1)$ (or θ_2) at f_1. Thus the input admittance of the short-circuited shunt stub is $Y_{in2}(f) = 1/(jZ_2\tan\theta(f))$. By properly designing TL2, its admittance is also odd-symmetrical with respect to the center frequency of 2.2 GHz, and varies inversely as compared to the imaginary part of Y_{in1}. It can make the imaginary part close to zero. As analyzed above, the admittances after adding TL1 are conjugated at f_1 and f_2, which can be expressed as $G-jB$ and $G+jB$, respectively. In order to offset the imaginary part, the admittance of the short-circuited shunt stub should be

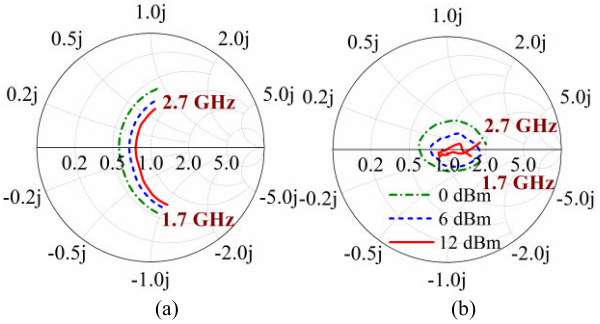

FIGURE 2. Input impedance (a) Z_{in1} with nearly odd-symmetrical imaginary part of the circuit with TL1 and (b) Z_R of the circuit with the impedance manipulation network from 1.7 to 2.7 GHz at different input power (0 dBm. 6 dBm, 12 dBm).

$$Y_{in2}(f_1) = \frac{1}{jZ_2\tan\theta_2} = jB \quad (5)$$

$$Y_{in2}(f_2) = \frac{1}{jZ_2\tan(k\theta_2)} = -jB. \quad (6)$$

Combining (5) and (6), we have the following relationship

$$\theta_2 = \frac{\pi}{1+k} \quad (7)$$

$$Z_2 = \frac{1}{B\tan(k\theta_2)}. \quad (8)$$

Therefore, the characteristic impedance Z_2 and electrical length θ_2 of TL2 can be calculated. In this design, Z_2 and θ_2 are 30.6 Ω and 69.6°, respectively. Fig. 2(b) depicts the input impedance Z_R of the rectifying circuit with the impedance manipulation network. As observed, the input impedance varying with frequency and power lies beside the real axis on Smith Chart. Therefore, the parameters Z_1, Z_2, θ_1, θ_2 for both two impedance manipulation networks can be calculated according to (3), (4), (7), and (8).

B. WIDEBAND RESISTANCE COMPRESSION NETWORK

In this part, a wideband RCN is proposed and applied to the rectifier design.

In a RCN, there are two transmission lines in the two branches of the RCN, with the electrical length of $90^0+\Delta\theta$ and $90^0-\Delta\theta$, respectively [27], and characteristic impedance Z_T. In order to develop it to wide band operation, firstly, the load of the RCN should be resistive in a wide band. This has been achieved by the impedance manipulation network. As analyzed above, by using the impedance manipulation network, the imaginary part of the rectifier input impedance

Z_R is close to zero, especially at the boundary frequencies f_1 and f_2. Thus it is negligible, and the real part of the input impedance is considered in the following analysis. Since the input resistance of the rectifier varies with input power, the common resistance range over the operating frequency band is denoted as $[Z_{R1}, Z_{R2}]$. According to the concept of RCN [29], we have

$$\frac{Z_T}{\tan(\Delta\theta)} = \sqrt{Z_{R1} \times Z_{R2}}. \tag{9}$$

In the conventional RCN, the electrical length of the two branches cannot remain complementary as frequency varies, resulting in a narrow frequency band. In this work, two coupled microstrip lines TL5 and TL6 are specifically designed to implement the wideband RCN as shown in Fig. 1 and 3. The characteristic impedance of TL5 is Z_{ce} for the even mode and Z_{co} for the odd mode, and its electrical length is θ_{C1} at f_1 and θ_{C2} at f_2. TL5 is equivalent to a transmission line with the characteristic impedance Z_T and electrical lengths θ_{T1} at f_1 and θ_{T2} at f_2. θ_{T1} is equal to $(90^0 + \Delta\theta)$. It is necessary to determine θ_{T1} and θ_{T2} to realize wideband resistance compression. They are expected to satisfy the following relationship

$$\theta_{T1} + \theta_{T2} = 180^\circ \tag{10}$$

In this case, TL6 is expected to be equivalent to a transmission line with the characteristic impedance Z_T, electrical length $(180^0 - \theta_{T1})$ at f_1, and electrical length θ_{T1} at f_2. Therefore, the equivalent electrical lengths of TL5 and TL6 remain complementary at f_1 and f_2, which satisfies the requirement of RCN.

The characteristic impedance and electrical length of the couple lines TL5 and TL6 are calculated based on θ_{T1}, θ_{T2} and Z_T, which are analyzed below.

The ABCD matrices of the coupled line TL5 and its equivalent transmission line satisfy the following relationship at f_1 [33]

$$\begin{bmatrix} \frac{Z_{ce} - Z_{co}\tan^2(\theta_{C1})}{Z_{ce} + Z_{co}\tan^2(\theta_{C1})} & \frac{2Z_{ce}Z_{co}j\tan(\theta_{C1})}{Z_{ce} + Z_{co}\tan^2(\theta_{C1})} \\ \frac{2j\tan(\theta_{C1})}{Z_{ce} + Z_{co}\tan^2(\theta_{C1})} & \frac{Z_{ce} - Z_{co}\tan^2(\theta_{C1})}{Z_{ce} + Z_{co}\tan^2(\theta_{C1})} \end{bmatrix} = \begin{bmatrix} \cos\theta_{T1} & jZ_T\sin\theta_{T1} \\ j\frac{\sin\theta_{T1}}{Z_T} & \cos\theta_{T1} \end{bmatrix}. \tag{11}$$

Then we have

$$\frac{Z_{ce} - Z_{co}\tan^2(\theta_{C1})}{Z_{ce} + Z_{co}\tan^2(\theta_{C1})} = \cos\theta_{T1} \tag{12}$$

$$\frac{2Z_{ce}Z_{co}j\tan(\theta_{C1})}{Z_{ce} + Z_{co}\tan^2(\theta_{C1})} = jZ_T\sin\theta_{T1} \tag{13}$$

$$\frac{2j\tan(\theta_{C1})}{Z_{ce} + Z_{co}\tan^2(\theta_{C1})} = j\frac{\sin\theta_{T1}}{Z_T}. \tag{14}$$

Likewise, the related expressions at f_2 can be obtained. Moreover, in order to satisfy (10), θ_{T1} and θ_{T2} are supposed

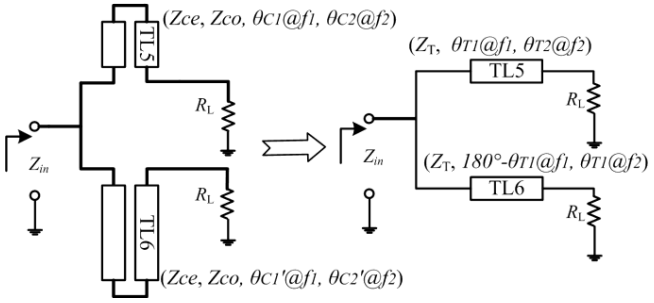

FIGURE 3. Proposed wideband RCN and its equivalent circuit.

to have the following relationship

$$\cos\theta_{T1} = -\cos\theta_{T2} \tag{15}$$

$$\sin\theta_{T1} = \sin\theta_{T2} \tag{16}$$

Combining (12) and (15), as well as (13) and (16), we have

$$Z_{ce} = Z_{ce}\tan\theta_{C1}\tan\theta_{C2} \tag{17}$$

Thus the odd- and even-mode characteristic impedance of TL5 can be calculated by combining (13), (14) and (17)

$$Z_{ce} = Z_T\sqrt{\tan\theta_{C1}\tan\theta_{C2}} \tag{18}$$

$$Z_{co} = \frac{Z_T}{\sqrt{\tan\theta_{C1}\tan\theta_{C2}}}. \tag{19}$$

After substituting (18) and (19) into (12), the electrical length of TL5 can be obtained by

$$\frac{\tan(\theta_{C2}) - \tan(\theta_{C1})}{\tan(\theta_{C2}) + \tan(\theta_{C1})} = \cos\theta_{T1} \tag{20}$$

where $\theta_{C2} = f_2/f_1 \times \theta_{C1}$ for TL5 with fixed physical length. Therefore, by solving (18)-(20), the characteristic impedance and electrical length of the coupled line TL5 are obtained. Subsequently, TL6 can also be designed according to the above equations, which has the equivalent characteristic impedance Z_T and electrical length $(180^0 - \theta_{T1})$ at f_1. In this way, the requirement of RCN can be satisfied at both the lower and upper frequencies f_1 and f_2. Moreover, the equivalent electrical length of the couple line TL5 changes from θ_{T1} to $(180^0 - \theta_{T1})$, while that of TL6 varies from $(180^0 - \theta_{T1})$ to θ_{T1} as the frequency increases from 1.7 to 2.7 GHz. In this case, the equivalent electrical length of TL5 and TL6 remains complementary to a certain extent over 1.7-2.7 GHz. Furthermore, because the input impedance of the rectifier changing with input power has similar variation range within the operating frequency band by using the impedance manipulation network, the resistance compression can be realized over the whole operating frequency band. Finally, TL7 is used to match the compressed impedance variation range to the antenna, which slightly improves the impedance matching performance. Note that if the proposed WRCN is applied to other rectifiers with extremely large or small diode impedance, such as the diode SMS7630, TL7 would be more useful.

C. CIRCUIT PERFORMANCE

Based on the above analysis and equations, a wideband RCN-based rectifier can be obtained. The rectifier is designed to work from 1.7 GHz to 2.7 GHz on the Rogers RO 4003 substrate, as shown in Fig. 4. The circuit parameters are optimized as: $L_1 = 2.6$ mm, $L_2 = 14.9$ mm, $L_3 = 7.6$ mm, $L_4 = 17.8$ mm, $L_5 = 5.85$ mm, $L_6 = 20.8$ mm, $L_7 = 10.7$ mm, $S = 1$ mm, $W_1 = 3.15$ mm, $W_2 = 2.1$ mm, $W_3 = 1$ mm, $W_4 = 1.7$ mm, $W_5 = 2.65$ mm, $W_6 = 5.4$ mm, $W_7 = 0.15$ mm. The 50 Ω-transmission line with the length of L5 is used to connect TL2 and TL5 (TL4 and TL6) in the layout of the rectifier, which slightly affects the performance.

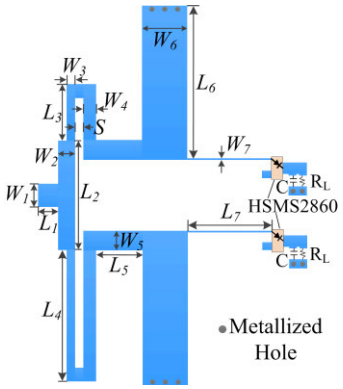

FIGURE 4. Geometry of proposed rectifier.

To highlight the advantage of wide operating power and frequency ranges of the proposed rectifier, three reference rectifiers as shown in Fig. 5 are compared, i.e.,

Rec1: a previous single-band rectifier with RCN by using the method in [29],
Rec2: a simple single-band rectifier without the RCN,
Rec3: a wideband rectifier without the RCN by using the method in [33].

Rec1 is realized by using a RCN [29]. Rec2 is completed by replacing the asymmetric RCN with a symmetric T-junction combiner. Rec3 is implemented by using two identical coupled lines and two impedance manipulation networks. Note that the function and design formulas of the couple lines in [33] is total different from the proposed wideband RCN. All the diodes used in the rectifiers are Schottky diode HSMS-2860, the capacitance value of the filtering capacitors is 100 pF, and the resistance value of loads is 510 Ω.

Fig. 6 shows the simulated S_{11} of the proposed wideband RCN-based rectifier, as well as the Rec1, Rec2, and Rec3. As observed, the proposed wideband RCN-based rectifier has a wider 15-dB impedance bandwidth of 1.5-2.7 GHz (57.1%) than Rec1 with a bandwidth of 1.9-2.45 GHz (25.3%). The frequency bandwidth of the proposed rectifier is similar with that of Rec3.

Fig. 7(a), (b) and (c) plot the S_{11} versus input power of all the rectifiers at 1.7 GHz, 2 GHz and 2.7 GHz, respectively. Note that Rec1 and Rec2 achieve the best matching at 2 GHz. As shown in Fig. 7 (b), the 15-dB return-loss power range

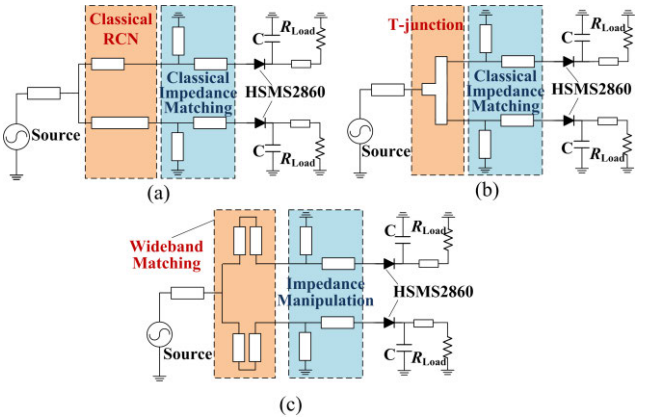

FIGURE 5. Three reference rectifiers (a) Rec1: a previous single-band rectifier with RCN in [29], (b) Rec2: a single-band rectifier without the RCN, (c) Rec3: a wideband rectifier without the RCN in [33].

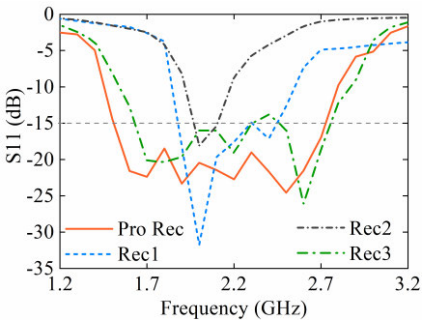

FIGURE 6. Simulated return loss of the proposed wideband RCN-based rectifier, as well as Rec1, Rec2, and Rec3 for the input power of 14 dBm.

of the proposed rectifier is similar with that of Rec1 at 2 GHz. Moreover, both Rec1 and the proposed one with RCNs achieve better impedance matching than Rec2 and Rec3 without RCNs. When the frequency varies, the matching performance of Rec1 and Rec2 is greatly degraded, as shown in Fig. 7 (a) and (c). However, the proposed rectifier still maintains good matching performance at 1.7 GHz and 2.7 GHz. Compared with Rec3, the proposed rectifier has wider operating power ranges, which means that the proposed rectifier achieves impedance compression in a wider frequency band.

For validation, the fabricated proposed rectifier is measured. The RF-DC conversion efficiency is quantified by

$$\eta(\%) = \frac{P_{\text{out1}} + P_{\text{out2}}}{P_{\text{in}}} \times 100 = \frac{V_{\text{out1}}^2 + V_{\text{out2}}^2}{R_L} \times \frac{1}{P_{\text{in}}} \times 100. \quad (21)$$

P_{in} is the input power. V_{out1} and V_{out2} are the output voltages of the rectifier, which are measured by two multimeters.

The simulated and measured efficiency of the proposed rectifier versus frequency is plotted in Fig. 8. The input power/frequency range for the conversion efficiency that is larger than 70% of peak efficiency is defined as the optimal power/frequency range. As seen, the optimal frequency

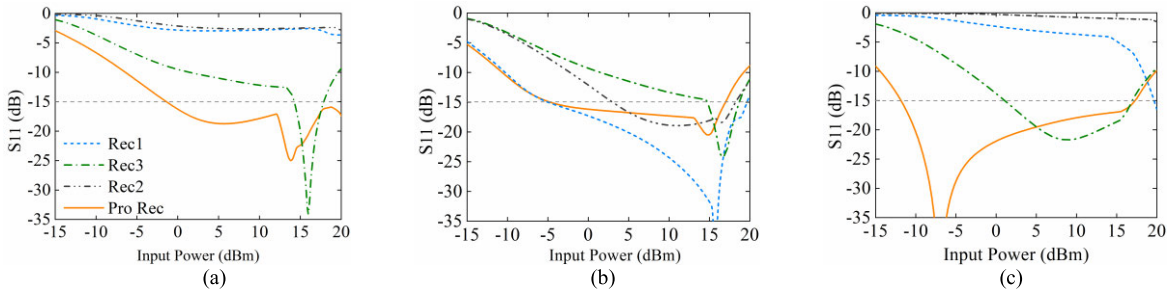

FIGURE 7. Simulated S_{11} of the proposed RCN-based rectifier, as well as Rec1, Rec2 and Rec3 at (a) 1.7 GHz, (b) 2 GHz, and (c) 2.7 GHz.

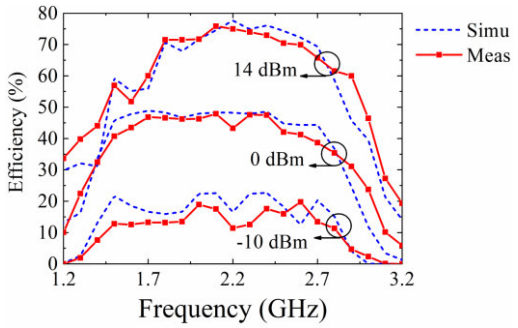

FIGURE 8. Simulated and measured efficiency of the proposed RCN-based rectifier for the input power of 14 dBm, 0 dBm and −10 dBm.

range includes the working frequency band of the broadband CP antenna is from 1.7 GHz to 2.7 GHz. The measured results agree well with the simulated ones. The slight difference is due to the fabrication tolerance and diode model inaccuracy.

Moreover, the comparison of the measured efficiency between the proposed rectifier and the Rec1, Rec2 and Rec3 is shown in Fig. 9. As shown in Fig. 9(a), four rectifiers have nearly equal peak efficiency for the input power of 14 dBm. But the proposed RCN-based rectifier and the Rec3 maintain high conversion efficiency in a much wider frequency band. When the input power decreases, as shown in Fig. 9(b) and (c), the measured efficiency of Rec2 and Rec3 without RCNs decreases substantially. When the input power is reduced to −10 dBm, the maximum efficiency of Rec2 and Rec3 is less than 5%, and that of the proposed rectifier is about 20%. This is because the input power variation results in not only the decrease of diode efficiency, but also the degradation of matching performance. The proposed RCN improves the impedance matching of the rectifier with a wide input power range, thereby increasing the efficiency. The proposed rectifier realizes impedance compression over a wide frequency range, thus improves the efficiency in a wide dynamic power and frequency range. The efficiency fluctuation of the rectifier is mainly due to the variation of impedance matching performance in the operating frequency band and the measurement error.

Furthermore, Fig. 10 illustrates the simulated and measured efficiency of the proposed rectifier and three reference ones versus input power at 2 GHz, which is the working frequency of Rec1 with RCN and Rec2 without RCN. The efficiency of Rec1 and the proposed rectifier with RCNs is higher than that of Rec2 and Rec3 without RCNs before the breakdown voltage is reached. Besides, the proposed rectifier has a comparable performance with Rec1, which indicates that the proposed method improves the bandwidth without scarifying the peak efficiency. It also can be seen that efficiency improvement of rectifiers at lower input power level (from −10 to 0 dBm) is larger than that with higher power level (from 0 to 14 dBm), which is caused by more serious impedance mismatch of the rectifier without RCN as input power decreases from the optimum power.

It should be noted that two branches in Fig. 4 can be combined into one output by connecting them in parallel with the load resistance of RL/2. In this case, the conversion efficiency remains almost unchanged.

D. COMPARISON

A comparison of the proposed rectifier with the wideband RCN with other related works reported in the literatures is given in Table 1. As observed, compared to other related works that extends the operating power range, the proposed rectifier achieves a wide operating power range and a much wider bandwidth. Moreover, compared with the ultra-wideband rectifier in [19], the proposed rectifier improves not only the frequency bandwidth, but also the operating power range since the proposed method improves the impedance matching when the input power varies. The proposed rectifier also has a comparable rectifier area with other works, except [32]. The reason for compact circuit area in [32] is that lumped components are used, which introduces much insertion loss at the same time. In addition, the proposed method also provides closed-form equations to clearly demonstrate the design of the rectifier. In brief, the rectifier using the proposed method can achieve high efficiency over wide dynamic power and frequency ranges.

Note that the WRCN-based rectifier with HSMS-2860 diodes in this work is designed as an example to prove the feasibility of the proposed method. The WRCN-based rectifier can work at lower or higher input power level by using appropriate diodes, such as the SMS-7630 diode with

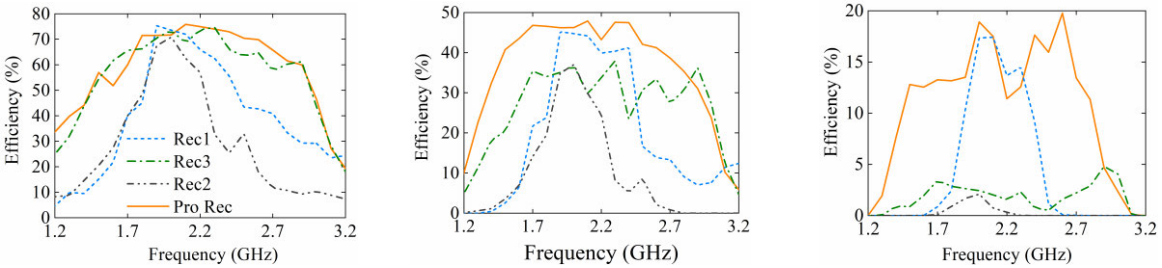

FIGURE 9. Measured efficiency of the proposed RCN-based rectifier, as well as Rec1, Rec2 and Rec3 for the input power of (a) 14 dBm, (b) 0 dBm, and (c) −10 dBm.

TABLE 1. Comparison with other related works.

TABLE I COMPARISON WITH OTHER RELATED WORKS

Ref	Type of diode	Maximum conversion efficiency	Freq. range/ Multi-band for efficiency (GHz) >60%	Input power level for efficiency >40 %	Rectifier area** (λ^2)
[6]	HSMS 2860	70 % at 1.85 GHz & 10 dBm	1, 1.82-1.98, 2.43	-2.5 to 15.5 dBm	N.A.
[19]	HSMS2862 +HSMS2852	85 % at 1.83 GHz & 12 dBm	1.47, 1.85, 2.19, 2.4	-8.5 to 17 dBm	N.A.
[25]	HSMS 286F	80.8 % at 2.45 GHz & 17.2 dBm	1.97-2.64	0 to 21.3 dBm	1.00*0.28 @2.45G Hz
[29]	HBAT 540B	70 % at 2.45 GHz & 27.3 dBm	2.45	19 dBm to N.A.	0.47*0.34 @2.45G Hz
[31]	HSMS 286F	76.2 % at 2.45 GHz & 18.1 dBm	2.27-2.6, 5.8	-1.5 to 22 dBm	0.53*0.53 @2.45G Hz
[32]	SMS 7630	75 % at 0.71 GHz & -1 dBm	0.51-0.55, 0.63-0.76, 0.92*	N.A.	0.1*0.06 @0.71G Hz
This work	**HSMS 2860**	**76 % at 2.1 GHz & 14 dBm**	**1.7-2.9**	**-3 to 20 dBm**	**0.41*0.25** @2.1GHz

* Simulated results.
** λ is the guided wavelength at the center frequency of the operating band.

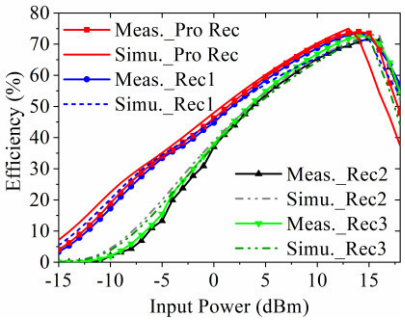

FIGURE 10. Measured and simulated efficiency of the proposed RCN-based rectifier, as well as Rec1, Rec2 and Rec3 versus input power at 2 GHz.

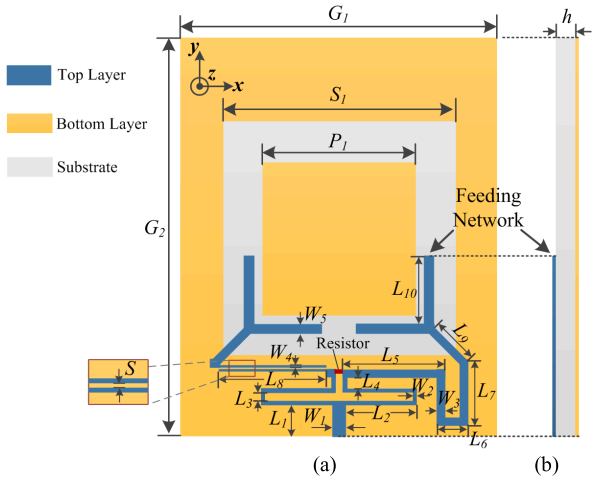

FIGURE 11. Geometry of proposed antenna: (a) top layer and bottom layer, and (b) side view.

low breakdown voltage (2 V) or HSMS-2820 diode with high breakdown voltage (15 V).

III. COMPACT BROADBAND CIRCULARLY POLARIZED ANTENNA DESIGN

The design of a compact and broadband CP antenna is proposed in this section. Based on [35], we employ a coupled-line-based phase shifter for wider operating bandwidth. It is used to receive RF energy for the rectifier in a wide frequency band. Simulated and measured results are also discussed, including S_{11}, axial ratio, gain and radiation patterns.

A. ANTENNA DESIGN

Fig. 11 shows the configuration of the proposed CP antenna which consists of a one-wavelength square-loop slot on the bottom layer of the substrate and a wideband feeding network on the top layer. The $1-\lambda$ loop-shaped radiating slot with a side-length of about $\lambda/4$ has more compact size and wider bandwidth than the conventional $\lambda/2$ rectangular radiating slot. It is very convenient to generate two orthogonal electric-field components by feeding the single loop-shaped radiating slot in orthogonal directions. The feeding network is composed of a microstrip feeding line, a Wilkinson power divider, a coupled-line-based 90^0 phase shifter and two Y-shaped feeding stubs. The characteristic impedance of the microstrip feeding line is $Z_0 = 50\ \Omega$. The power divider is implemented according to the procedure in [36]. The Wilkinson power divider have two $\lambda_g/4$-arms (λ_g is the guided wavelength in the center frequency) with a characteristic

impedance of $1.414Z_0$ for impedance transformation. There is a 100-Ω resistor palced across the outputs of the power divider. The coupled line with a gap and a uniform microstrip line without a gap together form a 90°-phase shifter. The coupled line can be used to enhance the operating bandwidth of the 90°-phase shifter according to [37]. The input RF signal is divided into two portions with the same magnitude and 90°-phase difference by the Wilkinson power divider and the 90°-phase shifter. They are fed to bottom corners of the loop slot by the corresponding Y-shaped feeding stubs. In this way, two orthogonal electric-field components with a phase difference of 90° are generated, and the proposed antenna can generate RHCP signal on one side and LHCP signal on the other side.

B. MEASUREMENT RESULTS

The broadband CP antenna is fabricated on the Rogers 4003 substrate ($\varepsilon_r = 3.38$, loss tangent: 0.0027) with an area of 56×75.5 mm^2. The antenna parameters are optimized as: $L_1 = 6.1$ mm, $L_2 = 10.5$ mm, $L_3 = 1.5$ mm, $L_4 = 2$ mm, $L_5 = 18$ mm, $L_6 = 5.5$ mm, $L_7 = 11.2$ mm, $L_8 = 19$ mm, $L_9 = 7.8$ mm, $L_{10} = 12$ mm, $S = 0.2$ mm, $W_1 = 2.5$ mm, $W_2 = 0.7$ mm, $W_3 = 1.5$ mm, $W_4 = 0.4$ mm, $W_5 = 1.8$ mm, $G_1 = 56$ mm, $G_2 = 75.5$ mm, $S_1 = 39$ mm, $P_1 = 29$ mm, $h = 1.524$ mm.

Fig. 12 depicts the measured and simulated S_{11}, axial-ratio (AR), and realized gain of the antenna. Fig. 12(a) shows that the antenna has a relative impedance bandwidth of 50.0% (1.68-2.8 GHz) for $S_{11} < -10$ dB. Fig. 12(b) shows that the AR bandwidth for AR < 3 dB is 48.4% (1.66-2.72 GHz). So the operating frequency bandwidth of the antenna is 1.68-2.72 GHz. Fig. 12(b) also shows the gain of the proposed antenna within the operating frequency band of 1.68-2.72 GHz ranges from 2.9 to 4.5 dBi. The gain variations of both simulation and measured results are less than 3 dB in the whole operating band, which is very desirable. Fig. 13 shows the normalized measured and simulated radiation patterns in the yz and xz planes at 1.7 GHz, 2.2 GHz and 2.7 GHz, whose radial scale of the normalized pattern is 10 dB. The proposed antenna radiates right-hand CP (RHCP) fields in the $+z$ axis direction, which is stronger than the left-hand CP (LHCP) fields (cross-polarization) by more than 10 dB across the whole band. Meanwhile, the antenna radiates LHCP fields in the $-z$ axis direction with 10 dB stronger than the RHCP fields (cross-polarization). The measurement results agree well with the simulaiton ones.

The CP antenna in [38] has much larger size than the proposed antenna. The antennas presented in [39], [40] are not suitable to be integrated with the proposed RCN, although they have wider operating bandwidth than the proposed one in this paper. It is because that the CP performance of the antennas in [39]–[41] is substantially affected by the current on the ground planes. If they are integrated with the RCN, the shapes and size of their ground planes will be changed a lot, and the current on the ground will also be changed deteriorating the CP performance. Therefore, the proposed antenna has comparable bandwidth and total size, and is suitable to be used to design a rectenna.

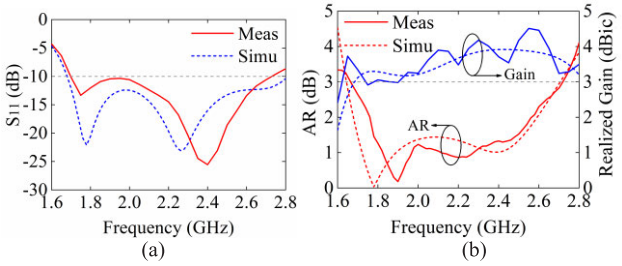

FIGURE 12. (a) Measured and simulated S_{11} (b) Measured and simulated AR and realized gain.

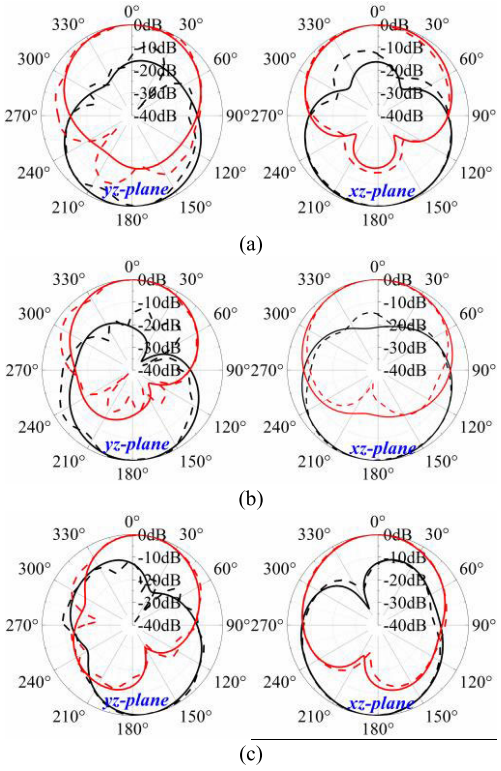

FIGURE 13. Measurement and simulation of the normalized radiation patterns at (a) 1.7 GHz, (b) 2.2 GHz, and (c) 2.7 GHz. (——: Simu._RHCP; ——: Simu._LHCP; - - -: Meas._RHCP; - — -: Meas._LHCP)

IV. BROADBAND RECTENNA BASED ON WIDEBAND RESISTANCE COMPRESSION TECHNIQUE

A. DESIGN OF THE RECTENNA

A broadband rectenna with wide dynamic operating power range is designed based on the above-mentioned CP antenna and rectifier. The designs of the CP antenna and rectifier were simulated by Driven Model in HFSS and harmonic balance (HB) simulation in ADS. Subsequently, the co-simulation between antenna and rectifier was performed in ADS by harmonic balance (HB) simulation. The proposed broadband CP antenna has a working frequency band of 1.68 - 2.72 GHz, and the wideband RCN-based rectifier

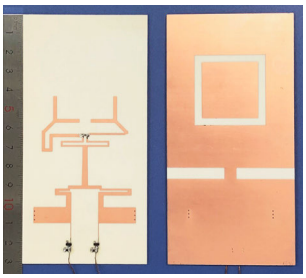

FIGURE 14. Photograph of the broadband rectenna based on the resistance compression technique.

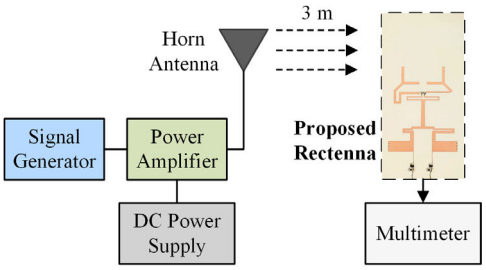

FIGURE 15. Diagram of the WPT system.

with a wide dynamic power range achieves more than 60% efficiency ($S_{11} < -15$ dB) in the frequency range of 1.7 - 2.7 GHz. The rectenna can be designed by slight optimization of the matching network between the antenna and rectifier. The rectifier is placed on the bottom layer of the antenna.

Fig. 14 shows the photograph of the broadband rectenna with a wide dynamic power range. A rectangular-loop slot lies on the top layer of the rectenna as the radiator. A small metal pad is used to connect the ground of the antenna and that of the rectifier together to ensure that the radiation performance of the slot antenna is affected little. Besides, a feeding network and a rectifier based on the wideband RCN are located on the bottom layer.

The diagram and photograph of the measurement WPT system for the rectenna are shown in Fig. 15 and Fig. 16. The RF signal is generated by the signal source, then amplified by the power amplifier with DC power supply and radiated by the horn antenna with left-handed circular polarization (HD-1040SGACPH7HL). Subsequently, it is harvested and rectified by the proposed rectenna, as well as being transmitted to the load. Finally, the output voltage is measured by a multimeter. The rectenna is located in the far field of the transmitting antenna with a transmission distance of 3 m. The RF-DC conversion efficiency of the rectenna is calculated by

$$\eta_{RF-dc} = \frac{P_{dc}}{P_r} \times 100\% = \frac{V_{\text{out1}}^2 + V_{\text{out2}}^2}{R_{\text{Load}} P_d A_{\text{eff}}} \times 100\%. \quad (22)$$

where V_{out1} and V_{out2} are the measured output voltages on the DC loads. P_d is the input power density and A_{eff} is the effective aperture size of the proposed rectenna. P_d is calculated by the Friss transmission equation as presented below.

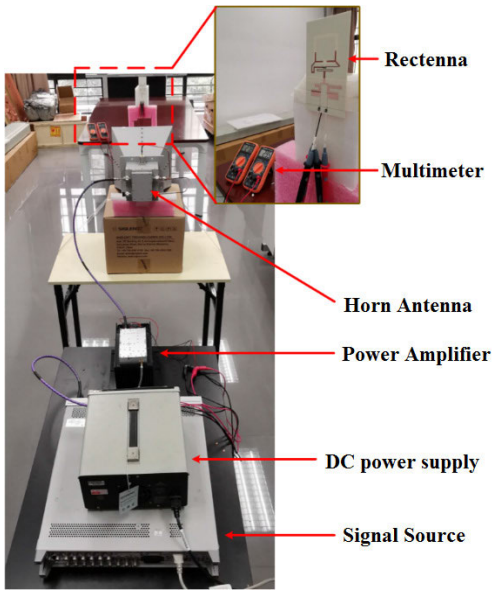

FIGURE 16. Experimental setup of WPT system.

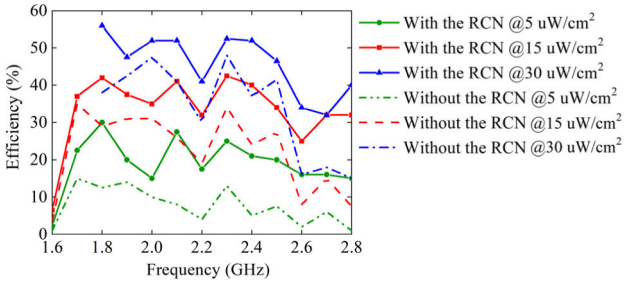

FIGURE 17. Measured RF-DC conversion efficiency of the rectennas with and without the wideband RCN for the power densities of 5 μ W/cm^2, 15μ W/cm^2, and 30μ W/cm^2.

$$P_d = \frac{P_t G_t}{4\pi D^2} \quad (23)$$

where P_t is the transmitting power, G_t is the horn antenna gain, and D is the distance between the horn antenna and the center of the rectenna. The attenuation of the system can also be calculated.

B. EXPERIMENTAL RESULTS

The measured efficiency of the broadband rectenna with and without the wideband RCN for the power density of 5 μW/cm^2, 15 μW/cm^2 and 30 μW/cm^2 is shown in Fig. 17. It can be seen that the RF-DC conversion of the rectenna is increased over a wide frequency band by using the proposed wideband RCN. Within the power density from 5 to 30 μW/cm^2, the efficiency improvement is up to about 24.5%. On the other hand, the efficiency of the rectenna increases with the power density. The fluctuations in efficiency are mainly due to slight instability of the measurement WPT system.

V. CONCLUSION

A novel wideband resistance compression technique has been proposed to improve the impedance matching performance between the rectifier and antenna, consequently increasing the conversion efficiency in wide operating power and frequency ranges. The proposed rectifier has achieved over 60% (up to 76%) conversion efficiency for the input power from 5 to 17 dBm and frequency bandwidth of 1.7-2.9 GHz. Compared with the previous RCN-based rectifiers, the proposed rectifier has achieved impedance compression and efficiency improvement in a wider frequency range. The proposed rectifiers have better conversion efficiency. The rectifier has also been co-designed with a broadband CP antenna working from 1.68 to 2.72 GHz to construct a broadband CP rectenna with dynamic-power-range. The proposed rectenna is of good industrial value as it can overcome the efficiency degradation of the WPT applications caused by the transmission distance and environmental changes to some extent. Also, it is able to be used among different countries and areas due to its wide operating band. In addition, the feeding network of the antenna and the matching network of the rectifier will be co-designed to miniaturize the rectenna in our future research. Moreover, antennas with higher gain will be designed to improve the received power of the rectenna.

REFERENCES

[1] M. R. Elhebeary, M. A. A. Ibrahim, M. M. Aboudina, and A. N. Mohieldin, "Dual-source self-start high-efficiency microscale smart energy harvesting system for IoT," *IEEE Trans. Ind. Electron.*, vol. 65, no. 1, pp. 342–351, Jan. 2018.

[2] C. Song, A. Lopez-Yela, Y. Huang, D. Segovia-Vargas, Y. Zhuang, Y. Wang, and J. Zhou, "A novel quartz clock with integrated wireless energy harvesting and sensing functions," *IEEE Trans. Ind. Electron.*, vol. 66, no. 5, pp. 4042–4053, May 2019.

[3] E. Moradi, L. Sydanheimo, G. S. Bova, and L. Ukkonen, "Measurement of wireless power transfer to deep-tissue RFID-based implants using wireless repeater node," *IEEE Antennas Wireless Propag. Lett.*, vol. 16, pp. 2171–2174, 2017.

[4] A. Costanzo and D. Masotti, "Energizing 5G: Near- and far-field wireless energy and data trantransfer as an enabling technology for the 5G IoT," *IEEE Microw. Mag.*, vol. 18, no. 3, pp. 125–136, May 2017.

[5] K. Huang and E. Larsson, "Simultaneous information and power transfer for broadband wireless systems," *IEEE Trans. Signal Process.*, vol. 61, no. 23, pp. 5972–5986, Dec. 2013.

[6] C. Song, Y. Huang, J. Zhou, P. Carter, S. Yuan, Q. Xu, and Z. Fei, "Matching network elimination in broadband rectennas for high-efficiency wireless power transfer and energy harvesting," *IEEE Trans. Ind. Electron.*, vol. 64, no. 5, pp. 3950–3961, May 2017.

[7] C. Song, Y. Huang, P. Carter, J. Zhou, S. Yuan, Q. Xu, and M. Kod, "A novel six-band dual CP rectenna using improved impedance matching technique for ambient RF energy harvesting," *IEEE Trans. Antennas Propag.*, vol. 64, no. 7, pp. 3160–3171, Jul. 2016.

[8] V. Palazzi, J. Hester, J. Bito, F. Alimenti, C. Kalialakis, A. Collado, P. Mezzanotte, A. Georgiadis, L. Roselli, and M. M. Tentzeris, "A novel ultra-lightweight multiband rectenna on paper for RF energy harvesting in the next generation LTE bands," *IEEE Trans. Microw. Theory Techn.*, vol. 66, no. 1, pp. 366–379, Jan. 2018.

[9] M. M. Mansour and H. Kanaya, "High-efficient broadband CPW RF rectifier for wireless energy harvesting," *IEEE Microw. Wireless Compon. Lett.*, vol. 29, no. 4, pp. 288–290, Apr. 2019.

[10] F. Bolos, D. Belo, and A. Georgiadis, "A UHF rectifier with one octave bandwidth based on a non-uniform transmission line," in *IEEE MTT-S Int. Microw. Symp. Dig.*, May 2016, pp. 15–64.

[11] J. Kimionis, A. Collado, M. M. Tentzeris, and A. Georgiadis, "Octave and decade printed UWB rectifiers based on nonuniform transmission lines for energy harvesting," *IEEE Trans. Microw. Theory Techn.*, vol. 65, no. 11, pp. 4326–4334, Nov. 2017.

[12] M. M. Mansour and H. Kanaya, "Compact and broadband RF rectifier with 1.5 octave bandwidth based on a simple pair of L-Section matching network," *IEEE Microw. Wireless Compon. Lett.*, vol. 28, no. 4, pp. 335–337, Apr. 2018.

[13] D. I. Kim, J. H. Moon, and J. J. Park, "New SWIPT using PAPR: How it works," *IEEE Wireless Commun. Lett.*, vol. 5, no. 6, pp. 672–675, Dec. 2016.

[14] A. Collado and A. Georgiadis, "Optimal waveforms for efficient wireless power transmission," *IEEE Microw. Wireless Compon. Lett.*, vol. 24, no. 5, pp. 354–356, May 2014.

[15] A. J. Soares Boaventura, A. Collado, A. Georgiadis, and N. B. Carvalho, "Spatial power combining of multi-sine signals for wireless power transmission applications," *IEEE Trans. Microw. Theory Techn.*, vol. 62, no. 4, pp. 1022–1030, Apr. 2014.

[16] A. Georgiadis, A. Collado, and K. Niotaki, "Rectenna design and signal optimization for electromagnetic energy harvesting and wireless power transfer," *IEICE Trans. Electron.*, vol. E98.C, no. 7, pp. 608–612, 2015.

[17] A. Boaventura, D. Belo, R. Fernandes, A. Collado, A. Georgiadis, and N. B. Carvalho, "Boosting the efficiency: Unconventional waveform design for efficient wireless power transfer," *IEEE Microw. Mag.*, vol. 16, no. 3, pp. 87–96, Apr. 2015.

[18] C.-C. Lo, Y.-L. Yang, C.-L. Tsai, C.-S. Lee, and C.-L. Yang, "Novel wireless impulsive power transmission to enhance the conversion efficiency for low input power," in *IEEE MTT-S Int. Microw. Symp. Dig.*, May 2011, pp. 55–58.

[19] C. Song, Y. Huang, P. Carter, J. Zhou, S. D. Joseph, and G. Li, "Novel compact and broadband frequency-selectable rectennas for a wide input-power and load impedance range," *IEEE Trans. Antennas Propag.*, vol. 66, no. 7, pp. 3306–3316, Jul. 2018.

[20] V. Marian, C. Vollaire, J. Verdier, and B. Allard, "Potentials of an adaptive rectenna circuit," *IEEE Antennas Wireless Propag. Lett.*, vol. 10, pp. 1393–1396, 2011.

[21] C. J. Li and T. C. Lee, "2.4-GHz high-efficiency adaptive power harvester," *IEEE Trans. Very Large Scale Integ. (VLSI) Syst.*, vol. 22, no. 2, pp. 434–438, Feb. 2014.

[22] V. Marian, B. Allard, C. Vollaire, and J. Verdier, "Strategy for microwave energy harvesting from ambient field or a feeding source," *IEEE Trans. Power Electron.*, vol. 27, no. 11, pp. 4481–4491, Nov. 2012.

[23] S. H. Abdelhalem, P. S. Gudem, and L. E. Larson, "An RF–DC converter with Wide-Dynamic-Range input matching for power recovery applications," *IEEE Trans. Circuits Syst. II, Exp. Briefs*, vol. 60, no. 6, pp. 336–340, Jun. 2013.

[24] Z. Liu, Z. Zhong, and Y.-X. Guo, "Enhanced dual-band ambient RF energy harvesting with ultra-wide power range," *IEEE Microw. Wireless Compon. Lett.*, vol. 25, no. 9, pp. 630–632, Sep. 2015.

[25] X. Y. Zhang, Z.-X. Du, and Q. Xue, "High-efficiency broadband rectifier with wide ranges of input power and output load based on branch-line coupler," *IEEE Trans. Circuits Syst. I, Reg. Papers*, vol. 64, no. 3, pp. 731–739, Mar. 2017.

[26] Y. Han, O. Leitermann, D. A. Jackson, J. M. Rivas, and D. J. Perreault, "Resistance compression networks for radio-frequency power conversion," *IEEE Trans. Power Electron.*, vol. 22, no. 1, pp. 41–53, Jan. 2007.

[27] J. Xu and D. S. Ricketts, "An efficient, watt-level microwave rectifier using an impedance compression network (ICN) with applications in outphasing energy recovery systems," *IEEE Microw. Wireless Compon. Lett.*, vol. 23, no. 10, pp. 542–544, Oct. 2013.

[28] K. Niotaki, A. Georgiadis, A. Collado, and J. S. Vardakas, "Dual-band resistance compression networks for improved rectifier performance," *IEEE Trans. Microw. Theory Techn.*, vol. 62, no. 12, pp. 3512–3521, Dec. 2014.

[29] T. W. Barton, J. M. Gordonson, and D. J. Perreault, "Transmission line resistance compression networks and applications to wireless power transfer," *IEEE J. Emerg. Sel. Topics Power Electron.*, vol. 3, no. 1, pp. 252–260, Mar. 2015.

[30] Q. W. Lin and X. Y. Zhang, "Differential rectifier using resistance compression network for improving efficiency over extended input power range," *IEEE Trans. Microw. Theory Techn.*, vol. 64, no. 9, pp. 2943–2954, Sep. 2016.

[31] Z.-X. Du and X. Y. Zhang, "High-efficiency Single- and dual-band rectifiers using a complex impedance compression network for wireless power transfer," *IEEE Trans. Ind. Electron.*, vol. 65, no. 6, pp. 5012–5022, Jun. 2018.
[32] C. Song, Y. Huang, J. Zhou, and P. Carter, "Improved ultrawideband rectennas using hybrid resistance compression technique," *IEEE Trans. Antennas Propag.*, vol. 65, no. 4, pp. 2057–2062, Apr. 2017.
[33] Y. L. Lin, X. Y. Zhang, Z.-X. Du, and Q. W. Lin, "High-efficiency microwave rectifier with extended operating bandwidth," *IEEE Trans. Circuits Syst. II, Exp. Briefs*, vol. 65, no. 7, pp. 819–823, Jul. 2018.
[34] Y. Wu, W. Sun, S.-W. Leung, Y. Diao, and K.-H. Chan, "A novel compact dual-frequency coupled-line transformer with simple analytical design equations for frequency-depending complex load impedance," *Prog. Electromagn. Res.*, vol. 134, pp. 47–62, 2013.
[35] Y. Cao, X. Shi, Z. Tan, and T. Mo, "A compact and wideband circularly polarized slot antenna based on AMC for satellite communication," in *Proc. IEEE 5th Int. Symp. Electromagn. Compat. (EMC-Beijing)*, Beijing, China, Oct. 2017, pp. 1–3.
[36] D. M. Pozar, *Microwave Engineering*, 4th ed. Hoboken, NJ, USA: Wiley, 2012, ch. 7, pp. 328–332.
[37] X. Y. Pu, S. Y. Zheng, J. Liu, Y. Li, and Y. Long, "Novel multi-way broadband differential phase shifter with uniform reference line using coupled line structure," *IEEE Microw. Wireless Compon. Lett.*, vol. 25, no. 3, pp. 166–168, Mar. 2015.
[38] C.-H. Lee and Y.-H. Chang, "An improved design and implementation of a broadband circularly polarized antenna," *IEEE Trans. Antennas Propag.*, vol. 62, no. 6, pp. 3343–3348, Jun. 2014.
[39] M. Samsuzzaman, M. T. Islam, and M. J. Singh, "A compact printed monopole antenna with wideband circular polarization," *IEEE Access*, vol. 6, pp. 54713–54725, 2018.
[40] H. H. Tran, N. Nguyen-Trong, and A. M. Abbosh, "Simple design procedure of a broadband circularly polarized slot monopole antenna assisted by characteristic mode analysis," *IEEE Access*, vol. 6, pp. 78386–78393, 2018.
[41] U. Ullah and S. Koziel, "Design and optimization of a novel miniaturized low-profile circularly polarized wide-slot antenna," *J. Electromagn. Waves Appl.*, vol. 32, no. 16, pp. 2099–2109, Nov. 2018.

ZHI-XIA DU (Member, IEEE) received the B.S. degree in applied physics and the Ph.D. degree in information and communication engineering from the South China University of Technology, Guangzhou, China, in 2014 and 2019, respectively.

From 2017 to 2018, he was with the Applied Electromagnetics Research Group, University of California at San Diego, San Diego, CA, USA, as a Visiting Graduate. His current research interests include wireless power transfer, time-modulated metasurfaces, and microwave circuits.

Dr. Du was awarded the Best Student Paper Prize in the 2015 National Conference on Microwave and Millimeter Wave Technology (NCMMW).

SHAO FEI BO was born in Shanxi, China. He received the B.S. degree in information engineering from the South China University of Technology, Guangzhou, China, in 2018, where he is currently pursuing the Ph.D. degree in circuits and systems.

His current research interests include microwave rectifiers and antennas.

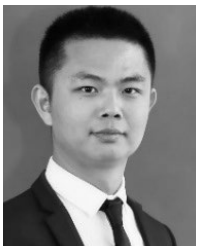

YUN FEI CAO (Member, IEEE) was born in Xinxiang, Henan, China, in 1990. He received the B.Eng. degree in information engineering from the South China University of Technology (SCUT), Guangzhou, China, in 2012, and the Ph.D. degree from the Department of Electrical and Electronic Engineering, The University of Hong Kong (HKU), Hong Kong, in 2016. He is currently an Associate Research Fellow with the School of Electronic and Information Engineering, SCUT. His current research interests include wireless power transfer, filtering antenna, reconfigurable antenna, and wearable antenna. He was a recipient of the Pearl River Talent Support Program for Postdoctoral Fellow.

JUN-HUI OU (Member, IEEE) received the B.E. degree in automation, the M.Sc. degree in communication engineering, and the Ph.D. degree in communication engineering from Sun Yat-sen University, Guangdong, China, in 2012, 2014, and 2018, respectively.

He holds a postdoctoral position at the South China University of Technology, Guangdong, China. He has published 16 EI/SCI recorded article. His current research interests include antenna design, RF circuit design, wireless power transmission, and simultaneous wireless information and power transmission.

XIU YIN ZHANG (Senior Member, IEEE) received the B.S. degree in communication engineering from the Chongqing University of Posts and Telecommunications, Chongqing, China, in 2001, the M.S. degree in electronic engineering from the South China University of Technology, Guangzhou, China, in 2006, and the Ph.D. degree in electronic engineering from the City University of Hong Kong, Hong Kong, in 2009.

From 2001 to 2003, he was with ZTE Corporation, Shenzhen, China. He was a Research Assistant, from July 2006 to June 2007, and a Research Fellow, from September 2009 to February 2010, with the City University of Hong Kong. He is currently a Full Professor and the Vice Dean with the School of Electronic and Information Engineering, South China University of Technology. He also serves as the Vice Director of the Guangdong Key Laboratory of Millimeter-Wave and Terahertz and the Vice Director of the Engineering Research Center for Short-Distance Wireless Communications and Network, Ministry of Education. He has authored or coauthored more than 140 internationally refereed journal articles (including more than 80 IEEE Transactions) and around 80 conference papers. His research interests include antennas and arrays, MMIC, microwave/terahertz circuits and sub-systems, and wireless communications.

Dr. Zhang is a Fellow of the Institution of Engineering and Technology. He was a recipient of the National Science Foundation for Distinguished Young Scholars of China, the Leading Talent of Technological Innovation of Ten-Thousands Talents Program, the Young Scholar of the Changjiang Scholars Program of Chinese Ministry of Education, and the Scientific and Technological Award (First Honor) of Guangdong Province. He has served as a General Chair/Technical Program Committee (TPC) Chair/ member and a Session Organizer/Chair for a number of conferences. He was the Supervisor of several conference best paper award winners.